



# Alloy modification for additive manufactured Ni alloy components Part II: Effect on subsequent machining properties

Lorenz Engelking<sup>1</sup> · Dirk Schroepfer<sup>1</sup> · Thomas Kannengiesser<sup>1</sup> · Antonia Eissel<sup>2</sup> · Kai Treutler<sup>2</sup> · Volker Wesling<sup>2</sup>

Received: 30 September 2022 / Accepted: 2 December 2022  
© The Author(s) 2022

## Abstract

Alloy 36 (1.3912) is an alloy with 36% nickel and 64% iron and is generally classified as a difficult-to-cut material. Increasingly complex structures and the optimization of resource efficiency are making additive manufacturing (AM) more and more attractive for the manufacture or repair of components. Subsequent machining of AM components is unavoidable for its final contour. By using modern, hybrid machining processes, e.g., ultrasonic-assisted milling (US), it is possible to improve the cutting situation regarding the resulting surface integrity as well as the cutting force. Part I deals with the influence of the alloying elements Ti, Zr, and Hf on the microstructure and the hardness of the initial alloy 36. Part II focusses on the effect of the alloy modifications and the ultrasonic assistance on machinability as well as on the surface integrity after finish-milling. The results show a highly significant influence of the ultrasonic assistance. The cutting force during the US is reduced by over 50% and the roughness of approx. 50% compared to conventional milling (CM) for all materials investigated. Moreover, the US causes a defect-free surface and induces near-surface compressive residual stresses. CM leads to a near-surface stress state of approx. 0 MPa.

**Keywords** Alloy 36 · Ultrasonic-assisted milling · Surface integrity · Modification of structural morphology

## 1 Introduction

In part I of this investigation, the initial alloy 36 is modified with the elements Ti, Zr, and Hf up to a maximum of 0.33 wt.-% [1]. The influence of the modification elements on the microstructure as well as on the hardness of the AM components is examined. Part II focusses on the effect of the alloy modifications on machinability as well as on the surface integrity of plasma-transferred-arc-welded (PTA) and finish-milled components made of alloy 36.

Alloy 36 (1.3912) with the trade name “Invar” is known for its very low coefficient of thermal expansion and was developed in 1897 by the Swiss scientist Charles Eduardo Guillaume [2]. Due to its high tendency for work hardening and low thermal conductivity, the alloy 36 is generally classified as a difficult-to-cut material [3]. The alloy is used to produce fiber-reinforced composites in the field of mold construction [4] or liquified natural gas (LNG) cargo tanks [5]. The sustained global trend towards energy efficiency and resource efficiency highlights the interest in additive manufacturing (AM). AM has multiple economic advantages in terms of component repair, modification, or manufacture [6] and is additionally characterized in particular by very efficient material utilization [7]. However, subsequent machining of these AM components, which is usually done by using a tool with a geometrically defined cutting edge (e.g., milling), is mandatory in order to realize the final contour or surface [8]. In addition, surface integrity plays an important role for safety-relevant components. It is determined by metallurgical (e.g., microstructure of the substrate), topological (e.g., surface defects, roughness), and mechanical (e.g., residual stresses) factors that are key to the safety and performance of the components [9]. Due to the thermal and mechanical

---

Recommended for publication by Commission II - Arc Welding and Filler Metals

- 
- ✉ Lorenz Engelking  
lorenz.engelking@bam.de
  - ✉ Antonia Eissel  
antonia.eissel@tu-clausthal.de

<sup>1</sup> Bundesanstalt für Materialforschung und -prüfung (BAM),  
Unter den Eichen 87, 12205 Berlin, Germany

<sup>2</sup> Institute of Welding and Machining (ISAF), Agricolastraße  
2, 38678 Clausthal-Zellerfeld, Germany

loads occurring during the subsequent machining process, tensile or compressive residual stresses are induced at the surface [10]. Compressive residual stresses have a beneficial effect on the resistance to corrosion fatigue [11], which plays an important role in LNG cargo tanks. In ultrasonic-assisted milling (US), the kinematic of conventional milling (CM) is superimposed with an axial oscillation of the milling tool in the ultrasonic range with an amplitude in the micrometer range. Rinck et al. carried out milling tests on Ti-6Al-4V. They found that US leads to an induction of compressive residual stresses at the surface as well as a reduced cutting force compared to CM [12]. Ni et al. observed for the same material a reduced cutting force and roughness caused by US compared to CM. Furthermore, they found a significantly reduced defect density on the milled surfaces with ultrasonic assistance compared to CM [13]. Su and Li investigated the influence of ultrasonic assistance on the resulting surface integrity of Ti-6Al-4V AM components manufactured via selective laser melting (SLM). They found an improved surface integrity in terms of roughness and surface quality of the AM components machined with ultrasonic assistance compared to CM [14]. Schroeffer et al. showed for specimens of a difficult-to-cut NiCrMo-alloy (IN725) manufactured via wire arc additive manufacturing (WAAM) a reduced cutting force as well as a reduced residual stress state by using US compared to CM [8]. By using modern, hybrid machining processes, e.g., US, it is possible to reduce the near-surface tensile residual stresses and even to induce compressive residual stresses. Moreover, the roughness as well as the defect density can be significantly reduced compared to CM. The microstructure has a direct influence on the cutting force as well as on the resulting surface integrity after machining [15]. Investigations on different materials show that a finer microstructure has a beneficial influence on the cutting force [15–17]. Furthermore, the grain size as well as the microstructure morphology has a significant positive influence on the cutting force when machining intermetallic polycrystalline materials [18]. Hard phases of the material cause a high load on the tool in the course of the machining process, as these strike the cutting edge at a high relative speed and lead to an impact load on the cutting edge, which results in high mechanical and thermal loads on the tool [19]. This is particularly true for the milling process, as it is a discontinuous cutting process.

**Table 1** Modifications of the FeNi36 initial alloy in wt.-%

Ti	0.1667	0	0	0.33	0	0	0.33	0	0.33	0.33
Zr	0	0.1667	0	0	0.33	0	0.33	0.33	0	0.33
Hf	0	0	0.1667	0	0	0.33	0	0.33	0.33	0.33

## 2 Methods

Machining tests were carried out on the PTA welds, to investigate the influence of ultrasonic assistance (power parameter  $P_{US}$  in %) and the effects of the modification elements Ti, Zr, and Hf on the occurring cutting forces, temperatures, and resulting surface integrity of the AM components made of alloy 36 (hereafter referred to as FeNi36) and their modifications, cf. Table 1. The experimental data is shown in Table 2.

The experimental setup of the finish-milling tests is shown in Fig. 1a. They were carried out in down milling mode and without cooling lubricant (dry conditions) on a 5-axis machining center (DMU 65 by DMG MORI) modified for ultrasonic-assisted milling. The milling tool (by WOLF Werkzeugtechnik GmbH) used was a PVD-coated (TiAlSiN) solid carbide ball end mill with four flutes and a diameter of 6 mm, which was tilted in the x- and in the y-direction by 45° each. The specimens with dimensions of approx. 15 mm × 15 mm × 2 mm (length × width × height) were extracted from the AM ingots by electrical discharge machining (EDM) as shown in Fig. 1b. The specimens were machined perpendicular to the build direction. The cutting speed was 30 m/min and the feed rate was 0.07 mm. The tests were performed once with and once without ultrasonic-assistance. One milling tool was used for each of the two machining processes. In total, 22 finish-milling experiments with two milling tools were carried out.

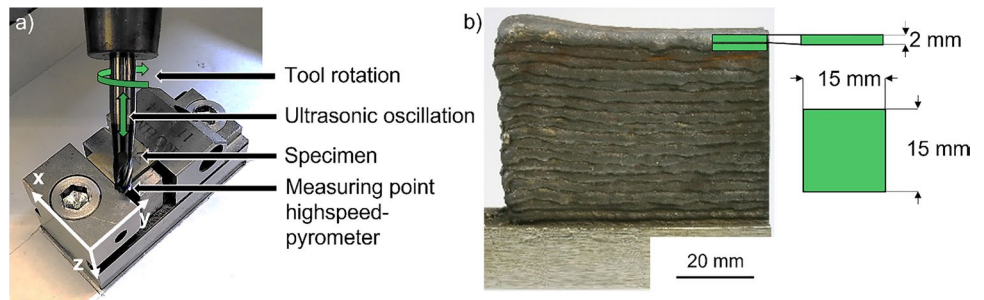
### 2.1 Temperature analysis

An in situ measurement of the temperature of the tool cutting edge (as the cutting edge passes through the air at the reversal point of the tool revolution) was realized using a high-speed pyrometer (KGA 740 by KLEIBER), cf. Figure 1a.

**Table 2** Experimental data for milling tests

Cutting speed $v_c = 30$ m/min	Feed rate $f_z = 0.07$ mm	Ultrasonic assistance $P_{US} = 0\%$ and 100%
Lead angle $\lambda = 45^\circ$	Step over $a_e = 0.3$ mm	Ultrasonic frequency $F_{US} = 41.75 \pm 0.15$ kHz
Tilt angle $\tau = 45^\circ$	Cutting engagement $a_p = 0.3$ mm	Ultrasonic amplitude $A_{US} = 8 \mu\text{m} \pm 1 \mu\text{m}$

**Fig. 1** **a** Experimental setup and **b** sampling and specimen dimension



## 2.2 Cutting force analysis

The cutting forces in x- (feed force  $F_f$ ), y- (feed normal force  $F_{fN}$ ) and z-direction (passive force  $F_p$ ) were measured in situ using a multicomponent dynamometer (by KISTLER, time resolution: 0.1 ms). The resulting cutting force  $F_{res}$  was calculated according to Eq. (1):

$$F_{res} = \sqrt{F_f^2 + F_{fN}^2 + F_p^2} \quad (1)$$

## 2.3 Roughness analysis

Roughness measurements were carried out using a light microscope (VHX-7000 by KEYENCE) with a measuring area of approx.  $1 \text{ mm}^2$  according to DIN EN ISO 25178–3 standard [20] with a stitching image of five times five images at  $1000\times$  magnification.

## 2.4 Residual stress analysis

The residual stresses were analyzed via X-ray diffraction (XRD) using a Goniometer G3 (by STRESSTECH) and  $\sin^2\psi$  method, cf. Table 3, to determine the effect of the cutting conditions. The analysis was performed in the center of the specimen  $0^\circ$ ,  $45^\circ$ , and  $90^\circ$  to the primary feed direction with a penetration depth of approx.  $5 \mu\text{m}$ . The calculations of the residual stresses were performed using the elastic moduli for alloy 36 ( $\nu = 0.25$ ;  $E = 140 \text{ GPa}$ ) [21]. The maximum principal residual stresses  $\sigma_{rs}^1$  were calculated according to [8].

## 3 Results and discussion

### 3.1 Temperature

For all materials investigated, the temperature of the tool cutting edge during air passing was below the lower limit of the measuring range of the highspeed pyrometer of  $160^\circ\text{C}$ . For other difficult-to-cut materials, e.g., a Co-Cr alloy, significantly higher temperatures were observed using the same experimental setup [22]. This observation leads to the conclusion that the temperatures of the tool cutting edge during the machining process are not critical for the tool for all materials investigated.

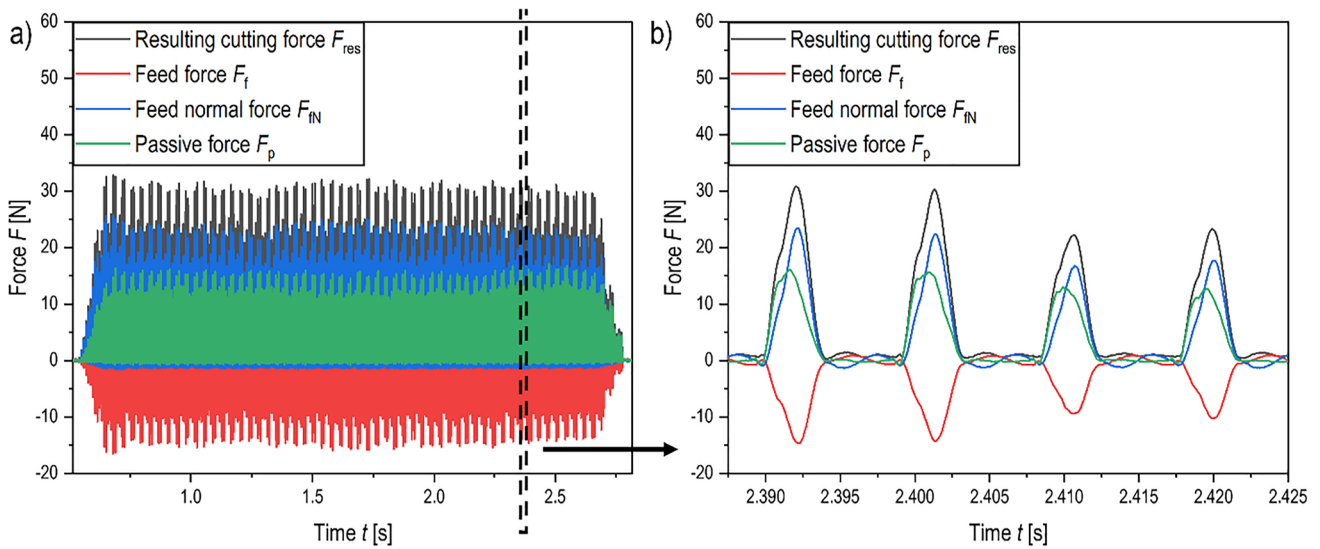
### 3.2 Cutting force

Figure 2 shows exemplarily the measured forces  $F_f$ ,  $F_{fN}$ , and  $F_p$  as well as the calculated resulting cutting force  $F_{res}$  for one milling line and one tool revolution. One peak represents one tooltip engagement each.

Figure 3a shows the resulting cutting force  $F_{res}$  as a function of the material for both processes. All modifications of the FeNi36 initial alloy investigated tend to increase the resulting cutting force for both machining processes. This effect can be explained by the hard precipitates formed by the respective modification element, cf. Part I [1]. Furthermore, for FeNi36, independent of the modification, US causes a significant reduction of the resulting cutting force by more than 50% compared to CM. The reduced friction between the workpiece and the milling tool and the interrupted cutting process due to the axial oscillation of the milling tool are decisive for this effect [12]. The reduced cutting forces in turn result in smaller load collectives for the workpiece and tool in US compared to CM. Figure 3b and

**Table 3** Parameters for XRD residual stress analysis

Measuring mode	Radiation	Detector	Diffraction line	$2\theta$ angle
$\sin^2\psi$	Mn-K $\alpha$	Linear solid-state	(311)	$152.3^\circ$
Collimator $\phi$	Tube power	$\psi$ -tilting	$\psi$ -step	Measuring time
3 mm	30 kV/6.7 mA	$0^\circ$ bis $\pm 45^\circ$	9	2 s



**Fig. 2** Exemplary representation of the cutting forces  $F_f$ ,  $F_{fN}$ , and  $F_p$  as well as the resulting cutting force  $F_{res}$  during milling: **a** one milling line; **b** one tool revolution

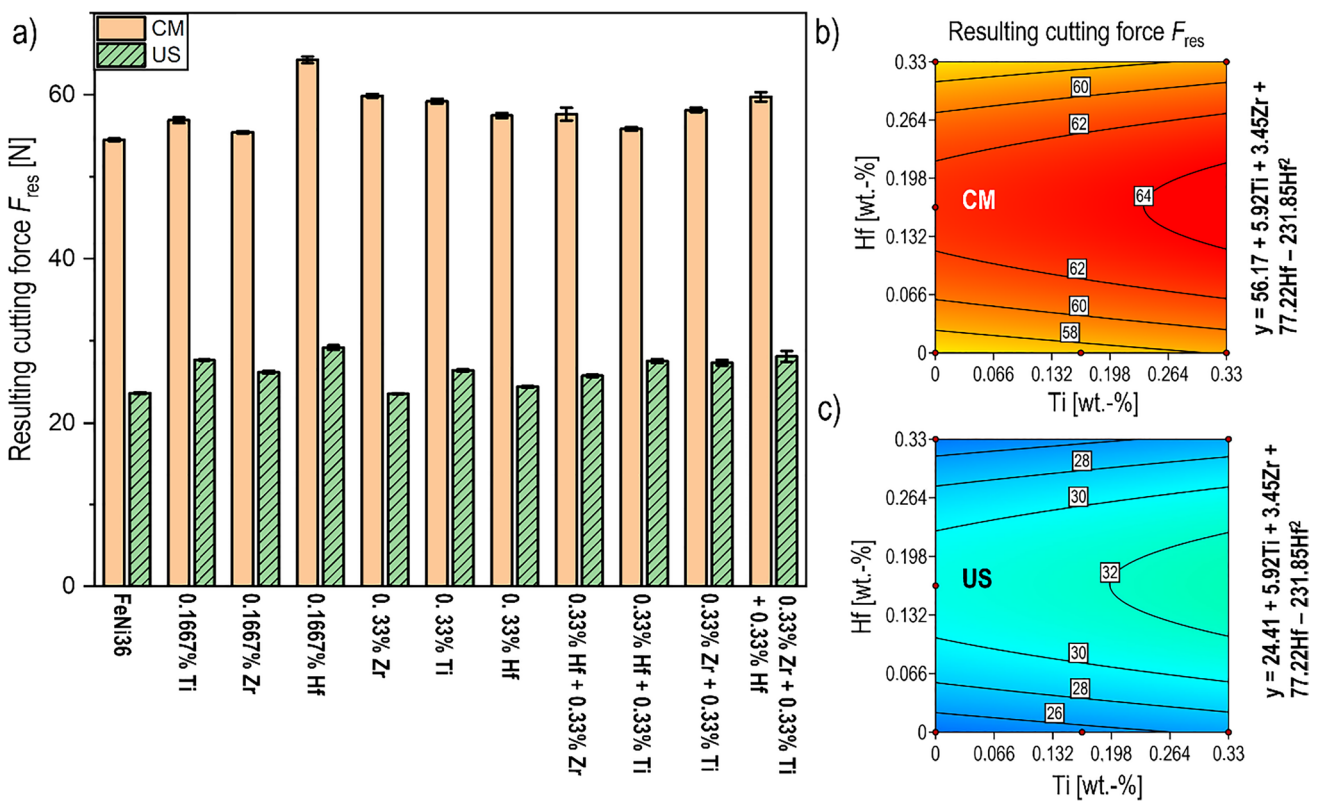


**Fig. 3** **a** Resulting cutting force  $F_{res}$  versus the material for conventional milling and ultrasonic assisted milling; resulting cutting force versus the modification elements Hf and Ti for **b** conventional milling and **c** ultrasonic assisted milling

**c** show the resulting cutting force as a function of the two modification elements Ti and Hf, Fig. 3b for CM, and Fig. 3c for US. Both diagrams are based on a regression model on basis of the design of experiments with a model quality of

$R^2=99\%$  given in the figures respectively. For both CM and US, a squared effect of the modification element Hf can be observed. Thus, modification of the FeNi36 initial alloy with an intermediate Hf content leads to the highest cutting forces

for both processes. It is assumed that the precipitates of the modification of the FeNi36 initial alloy with 0.33 wt.-% Hf compared to the modification with 0.1667 wt.-% Hf are more homogeneously distributed in the microstructure, which causes a more stable cutting process and ultimately leads to a lower cutting force. This assumption needs to be further investigated. Remarkable is the highly significant reduction of the process forces by using US.

### 3.3 Surface integrity

#### 3.3.1 Defect density

Figure 4a shows light microscope images of finish-milled surfaces for US and CM. It is remarkable that the US, in contrast to the CM, causes a significantly lower defect density and size, even to the point of avoiding such macroscopic defects. This can be attributed to the avoidance of a built-up edge (BUE). The high tendency for work hardening combined with the low thermal conductivity of the alloy FeNi36 causes a significant amount of the material adhering to the tooltip in the course of the finish-milling process and forms a so-called BUE [23]. In the further course of the milling process, the BUE sticks again to the surface and consequently causes a high degree of surface defects [24]. Due to the ultrasonic oscillation of the milling tool, the adhesion of the material to the tooltip is reduced which then consequently leads to an avoidance of the formation of a BUE. This effect is also reflected in the lower roughness values of the surface finish-milled with ultrasonic assistance compared to the surface machined with CM.

#### 3.3.2 Residual stress

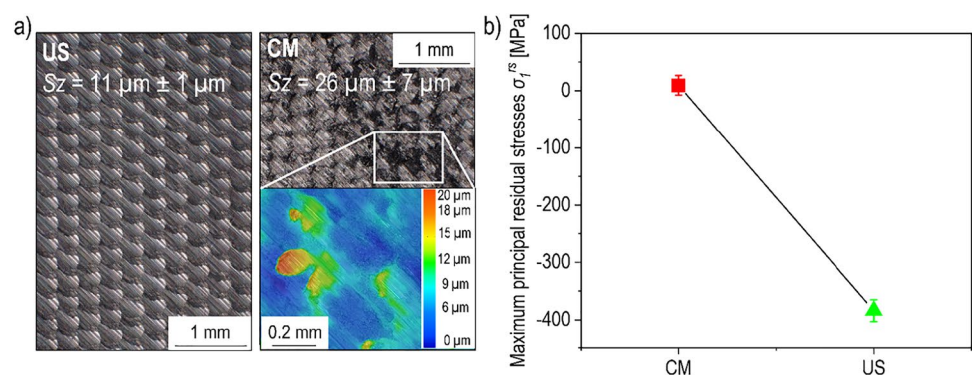
Figure 4b shows the near-surface maximum principal residual stress  $\sigma_{rs}^1$  as a function of the machining process for the finish-milled specimen made of the FeNi36 initial. The near-surface maximum principal residual stress of the specimen machined with CM is approx. 0 MPa due to the thermomechanical loads occurring during the finish-milling process.

US induces compressive residual stresses at the surface. An elastic strain of the workpiece surface occurs in the course of a compressive load caused by the ultrasonic oscillation of the tool, which leads to a local plastic deformation of the workpiece surface. After relief, the material that is underneath the indentation tries to return to its original shape. However, this is prevented by the surrounding material and compressive residual stresses are formed [11]. These compressive residual stresses even exceed the yield strength of the material [20], which can be explained by work hardening occurring during the milling process. Induction of near-surface compressive residual stresses caused by US was also observed for a modification of the FeNi36 initial alloy with 1.6 wt.-% Nb for a wide range of cutting parameters [25].

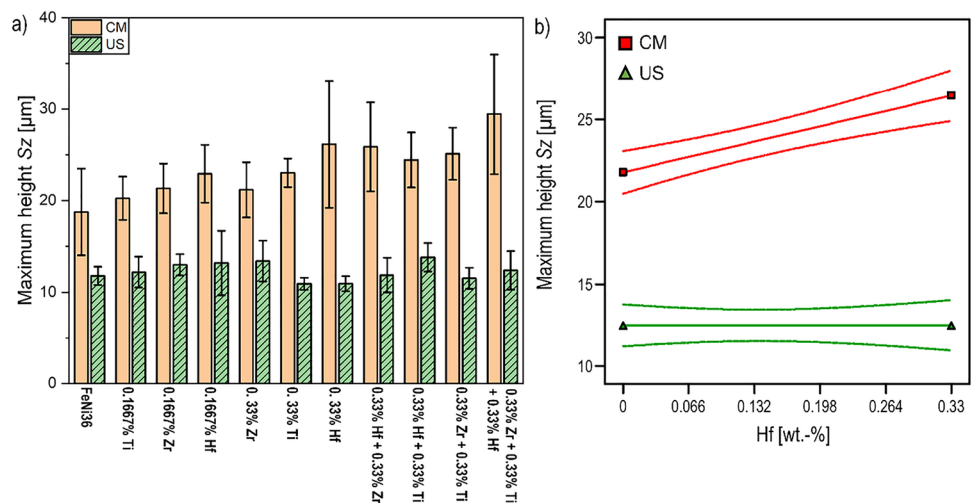
#### 3.3.3 Roughness

Figure 5a shows the maximum height  $S_z$  as a function of the material for both machining processes.  $S_z$  is defined as the sum of the largest value of the peak height and the largest value of the sink height within the defined measuring area [26]. All modifications of the FeNi36 initial alloy tend to increase the roughness of the finish-milled surfaces for CM compared to the finish-milled surface of the FeNi36 initial alloy. For US, the modifications have no significant influence on the roughness. It should be noted that, analogous to the observations made for the cutting forces, US causes a significant reduction in roughness of about 50% compared to CM. This effect can be explained again with the avoidance of the formation of a BUE, cf. Section 3.3.1. Figure 5b shows the roughness as a function of the modification element Hf for both machining processes. Analogous to the statistical evaluations of the cutting forces, it was possible to develop regression models based on the DoE, which shows the observed significant correlation between the content of alloying elements and the roughness of the material. A modification with Hf leads to an increase in the roughness compared to the FeNi36 initial alloy for CM. It can be supposed that, based on investigations on difficult-to-cut materials by Ranganath et al. and Liu et al., the appearance of

**Fig. 4** **a** Light microscope images of finish milled surfaces for US and CM and **b** maximum principal residual stress  $\sigma_{rs}^1$  vs. machining process (FeNi36 initial alloy)



**Fig. 5** Maximum height  $S_z$ : **a** versus the material and **b** versus the modification element Hf for conventional milling and ultrasonic-assisted milling



precipitates formed by Hf causes surface defects similar to carbide cracking [24, 27]. It is a common phenomenon in machining difficult-to-cut alloys [9, 24, 27, 28]. Due to the very low depth of cut (in this case 0.3 mm, which is a typical value for finishing) during a finish-milling process, carbides are deformed and eventually cracked or detached from the material and consequently result in surface defects and higher roughness values [27]. In contrast to the behavior of CM, no such influence can be observed for US caused by the modification with Hf. Overall, US appears to be less vulnerable to such defects due to microstructural characteristics such as precipitation. Due to the ultrasonic oscillation of the milling tool, there is less contact between the tool cutting edge and the precipitates which results in the avoidance of the deformation of these particles. Again, remarkable is the highly significant reduction of the roughness by using US.

## 4 Conclusion

Finish-milling tests were carried out on PTA welds of the FeNi36 initial alloy and its modifications with different concentrations of Ti, Hf, and Zr within an experimental design of experiments. The influence of the alloy modification and the use of ultrasonic assistance in the milling process on the resulting cutting forces and surface integrity were investigated. The following conclusions can be drawn:

- (1) The modification with Hf shows a squared effect on the resulting cutting force, the highest cutting force was observed with a medium modification with Hf of the FeNi36 initial alloy.
- (2) The modification with Hf causes an increase of the roughness for conventional milling compared to the FeNi36 initial alloy, which assumably stems from

machining the hard precipitates formed by the alloying element Hf.

- (3) The modifications of the initial FeNi36 alloy show a trend to increase the resulting cutting force as well as the roughness.
- (4) Compared to conventional milling, ultrasonic-assisted milling leads to a highly significant reduction of the cutting force during milling by over 50%, and to a considerably lower roughness of the milled surfaces by approx. 50% for all the initial alloy and all modifications.
- (5) Ultrasonic-assisted milling causes a defect-free surface compared to a surface with a very high defect density machined with conventional milling, which mainly can be traced back to an effective avoidance of build-up edge during milling as a result of the ultrasonic-oscillation of the tool tip during the cutting engagement.
- (6) Ultrasonic-assisted milling induces near-surface compressive residual stresses due to a local plastic deformation of the workpiece surface. These compressive residual stresses are beneficial regarding the resistance to corrosion fatigue.

**Acknowledgements** The IGF project IGF No. 20.979 N (DVS 01.3211) of the Research Association of the DVS was supported by the Federal Ministry for Economic Affairs and Climate Action by the AiF as part of the program for support of the cooperative industrial research (IGF) on the basis of a decision by the German Bundestag. We would like to thank for this funding and the companies involved in the project committee their support, in particular Deloro Wear Solutions GmbH, ECKART GmbH and S3 Handel und Dienstleistungen UG for providing the welding powder, WOLF Werkzeugtechnologie GmbH for providing the milling tools and DMG MORI Ultrasonic Lasertec GmbH for providing the ultrasonic actuator. In addition, we would like to thank Andreas Boerner and Sepehrdad Dorrani for their support in the milling experiments and analysis of the milled specimens.

**Funding** Open Access funding enabled and organized by Projekt DEAL.

**Data Availability** The datasets generated during and/or analysed during the current study are available from the corresponding author on reasonable request.

## Declarations

**Conflict of interest** The authors declare no competing interests.

**Open Access** This article is licensed under a Creative Commons Attribution 4.0 International License, which permits use, sharing, adaptation, distribution and reproduction in any medium or format, as long as you give appropriate credit to the original author(s) and the source, provide a link to the Creative Commons licence, and indicate if changes were made. The images or other third party material in this article are included in the article's Creative Commons licence, unless indicated otherwise in a credit line to the material. If material is not included in the article's Creative Commons licence and your intended use is not permitted by statutory regulation or exceeds the permitted use, you will need to obtain permission directly from the copyright holder. To view a copy of this licence, visit <http://creativecommons.org/licenses/by/4.0/>.

## References

- Eissel A, Engelking L, Gustus R, Treutler K, Wesling V, Schroepfer D, Kannengiesser T (2022) Alloy modification for additive manufactured Ni alloy components Part I: effect on microstructure and hardness. *Welding in the World* (under review)
- Sahoo A, Medicherla VRR (2021) Fe-Ni invar alloys: a review. *materials today: Proceedings* 43:2242–2244. <https://doi.org/10.1016/j.matpr.2020.12.527>
- Zheng XW, Ying GF, Lu J, Yang NH, Chen Y, Fu YC (2014) The influence of cutting parameters on the cutting forces when milling Invar36. *Adv Mater Res* 988:296–299. <https://doi.org/10.4028/www.scientific.net/AMR.988.296>
- Seeger M (2013) Entwicklung und Bewertung lichtbogen-gespritzter Invar-Laminier- und Vorrichtungen für die CFK-Produktion. München, Technische Universität München, Universitätsbibliothek der TU München, Diss. <https://mediatum.ub.tum.de/doc/1115864/1115864.pdf>. <https://nbn-resolving.de/urn/resolver.pl?urn:nbn:de:bvb:91-diss-20130225-1115864-0-2>
- Oh DJ, Lee JM, Kim MH (2014) Fatigue strength assessment of Invar alloy weld joints using the notch stress approach. *Eng Fail Anal* 42:87–99. <https://doi.org/10.1016/j.engfailanal.2014.04.003>
- Treutler K, Wesling V (2021) The current state of research of wire arc additive manufacturing (WAAM): a review. *Appl Sci* 11(18). <https://doi.org/10.3390/app11188619>
- Ding D, Pan Z, Cuiuri D, Li H (2015) Wire-feed additive manufacturing of metal components: technologies, developments and future interests. *Int J Adv Manuf Technol* 81(1–4):465–481. <https://doi.org/10.1007/s00170-015-7077-3>
- Schroepfer D, Treutler K, Boerner A, Gustus R, Kannengiesser T, Wesling V, Maus-Friedrichs W (2021) Surface finishing of hard-to-machine cladding alloys for highly stressed components. *Int J Adv Manuf Technol* 114(5–6):1427–1442. <https://doi.org/10.1007/s00170-021-06815-y>
- Ulutan D, Ozel T (2011) Machining induced surface integrity in titanium and nickel alloys: a review. *Int J Mach Tools Manuf* 51(3):250–280. <https://doi.org/10.1016/j.ijmachtools.2010.11.003>
- Ma Y, Feng P, Zhang J, Wu Z, Yu D (2016) Prediction of surface residual stress after end milling based on cutting force and temperature. *J Mater Process Technol* 235:41–48. <https://doi.org/10.1016/j.jmatprotec.2016.04.002>
- Meo M, Vignjevic R (2003) Finite element analysis of residual stress induced by shot peening process. *Adv Eng Softw* 34(9):569–575. [https://doi.org/10.1016/s0965-9978\(03\)00063-2](https://doi.org/10.1016/s0965-9978(03)00063-2)
- Rinck PM, Gueray A, Kleinwort R, Zaeh MF (2020) Experimental investigations on longitudinal-torsional vibration-assisted milling of Ti-6Al-4V. *Int J Adv Manuf Technol* 108(11–12):3607–3618. <https://doi.org/10.1007/s00170-020-05392-w>
- Ni C, Zhu L, Liu C, Yang Z (2018) Analytical modeling of tool-workpiece contact rate and experimental study in ultrasonic vibration-assisted milling of Ti-6Al-4V. *Int J Mech Sci* 142–143:97–111. <https://doi.org/10.1016/j.ijmecsci.2018.04.037>
- Su Y, Li L (2022) Surface integrity of ultrasonic-assisted dry milling of SLM Ti6Al4V using polycrystalline diamond tool. *Int J Adv Manuf Technol* 119(9–10):5947–5956. <https://doi.org/10.1007/s00170-022-08669-4>
- Pan Z, Feng Y, Liang SY (2017) Material microstructure affected machining: a review. *Manuf Rev* 4. <https://doi.org/10.1051/mfreview/2017004>
- Dang J, Cai X, Yu D, An Q, Ming W, Chen M (2019) Effect of material microstructure on tool wear behavior during machining additively manufactured Ti6Al4V. *Archiv Civ Mech Eng* 20(1). <https://doi.org/10.1007/s43452-019-0007-7>
- Denkena B, Grove T (2016) The effect of microstructure on the machinability of Ti-6Al-4V. *Proceedings of the 13th World Conference on Titanium:905–910*. <https://doi.org/10.1002/978119296126.ch155>
- Venkatachalam S, Fergani O, Li X, Guo Yang J, Chiang K-N, Liang SY (2015) Microstructure effects on cutting forces and flow stress in ultra-precision machining of polycrystalline brittle materials. *J Manuf Sci Eng* 137(2). <https://doi.org/10.1115/1.4029648>
- Weinert K, Buschka M, Hesterberg S (2001) Drehen und Fräsen pulvermetallurgischer Hartlegierungen für warmgehende Werkzeuge. *Materialwiss Werkstofftech* 32(5):434–446. [https://doi.org/10.1002/1521-4052\(200105\)32:5%3c434::Aid-mawe434%3e3.0.Co;2-w](https://doi.org/10.1002/1521-4052(200105)32:5%3c434::Aid-mawe434%3e3.0.Co;2-w)
- Beuth (2012) DIN EN ISO 25178-3:2012-11. Geometrische Produktspezifikation (GPS) - Oberflächenbeschaffenheit: Flächenhaft - Teil 3: Spezifikationsoperatoren (ISO 25178-3:2012); Deutsche Fassung EN ISO 25178-3:2012. <https://doi.org/10.31030/1876351>
- Corporation SM (2004) The NILO® and NILOMAG® Nickel-Iron Alloys. Publication Number SMC-031. <https://www.specialmetals.com/documents/technical-bulletins/nilo-alloys.pdf>
- Engelking L, Eissel A, Schroepfer D, Treutler K, Kannengiesser T, Wesling V (2021) Untersuchungsmethoden beim Fräsen additiv gefertigter schwer spanbarer Kobalt-Chrom-Legierungen. In: Brockmann S, Krupp U (eds) *Stahlinstitut VDEh, Düsseldorf, Tagung Werkstoffprüfung 2021, Online, 2021*, pp 93–98
- Ahmed YS, Fox-Rabinovich G, Paiva JM, Wagg T, Veldhuis SC (2017) Effect of built-up edge formation during stable state of wear in AISI 304 stainless steel on machining performance and surface integrity of the machined part. *Materials (Basel)* 10(11). <https://doi.org/10.3390/ma10111230>
- Liu C, Ren C, Wang G, Yang Y, Zhang L (2015) Study on surface defects in milling Inconel 718 super alloy. *J Mech Sci Technol* 29(4):1723–1730. <https://doi.org/10.1007/s12206-015-0345-1>
- Engelking L, Eissel A, Schroepfer D, Treutler K, Kannengiesser T, Wesling V (2022) Additive Fertigung – Werkstoffe – Prozesse – Wärmebehandlung 2022 - Tagungsband. In: Fechte-Heinen R, Bielefeld T (eds) *Additive Fertigung – Werkstoffe – Prozesse – Wärmebehandlung 2022, Bremen, 29.06.2022 - 30.06.2022*. Arbeitsgemeinschaft Wärmebehandlung und Werkstofftechnik e. V., pp 57–67

26. Beuth (2012) DIN EN ISO 25178-2:2012-09. Geometrische Produktspezifikation (GPS) - Oberflächenbeschaffenheit: Flächenhaft - Teil 2: Begriffe und Oberflächen-Kenngrößen (ISO 25178-2:2012); Deutsche Fassung EN ISO 25178-2:2012. <https://doi.org/10.31030/1754208>
27. Ranganath S, Guo C, Holt S (2009) Experimental investigations into the carbide cracking phenomenon on Inconel 718 superalloy material. In: ASME 2009 International Manufacturing Science and Engineering Conference, pp 33–39. <https://doi.org/10.1115/msec2009-84085>
28. Thakur A, Gangopadhyay S (2016) State-of-the-art in surface integrity in machining of nickel-based super alloys. *Int J Mach Tools Manuf* 100:25–54. <https://doi.org/10.1016/j.ijmachtools.2015.10.001>

**Publisher's note** Springer Nature remains neutral with regard to jurisdictional claims in published maps and institutional affiliations.